Supporting Information

Self-programming Synaptic Resistor Circuit for Intelligent Systems

*Christopher M. Shaffer, Atharva Deo, Andrew Tudor, Rahul Shenoy, Cameron D. Danesh, Dhruva Nathan, Lawren L. Gamble, Daniel J. Inman, and Yong Chen**

Spike-timing-dependent plasticity learning algorithm in a neurological network

In a neural network, the matrix of synaptic weights (conductances), $\boldsymbol{w}$, is modified in parallel based on synaptic spike-timing-dependent plasticity[1] (STDP), which can be expressed as $\dot{\boldsymbol{w}} = \alpha\, \boldsymbol{z} \otimes \boldsymbol{x}$ (Equation 2), where $\boldsymbol{x}$ denotes voltage pulses in the presynaptic neurons, and $\boldsymbol{z}$ is a function of $\boldsymbol{y}$ that represents voltage pulses in the postsynaptic neurons,

$$\boldsymbol{z} = \boldsymbol{y} * \tilde{\theta} \qquad \text{(S1)}$$

where $\boldsymbol{y} * \tilde{\theta} = \int_{-\infty}^{\infty} \tilde{\theta}(t - t')\boldsymbol{y}(t')dt'$ with $\tilde{\theta}(t) = \begin{cases} -e^{t/\tau_-}/\tau_- & when\ t < 0 \\ 0 & when\ t = 0 \\ e^{-t/\tau_+}/\tau_+ & when\ t > 0 \end{cases}$, and the time constants $\tau_+ > 0$ and $\tau_- > 0$. $\int_{-\infty}^{\infty} \tilde{\theta}(t)dt = 0$, thus $\int_{-\infty}^{\infty} \boldsymbol{z}(t)dt = 0$. By substituting $\boldsymbol{z} = \boldsymbol{y} * \tilde{\theta}$ (Equation S1) in Equation 2, $\dot{w}_{nm} = \sum_{t_n} \begin{cases} -\alpha\, x_m(t)\, e^{\frac{t-t_n}{\tau_-}}/\tau_- & when\ t < t_n \\ 0 & when\ t = t_n \\ \alpha\, x_m(t) e^{-\frac{t-t_n}{\tau_+}}/\tau_+ & when\ t > t_n \end{cases}$, where t_n denotes the moment t_n when a voltage pulse is triggered from the n[th] postsynaptic “neuron”, $\alpha > 0$ for STDP, and $\alpha < 0$ for anti-STDP.

Modeling and analysis of self-programming processes

The goal of the self-programming process is to modify the system state, $\boldsymbol{F}$, toward the desired system state, $\widehat{\boldsymbol{F}}$, and minimize the objective function $E = \frac{1}{2}(\boldsymbol{F} - \widehat{\boldsymbol{F}})^2$. When $\boldsymbol{F} = \widehat{\boldsymbol{F}}$, $E = 0$, $\boldsymbol{x} = 0$, and $\dot{\boldsymbol{w}} = \alpha\, \boldsymbol{z} \otimes \boldsymbol{x} = 0$ (Equation 2), $\boldsymbol{w}$ reaches an equilibrium value $\widehat{\boldsymbol{w}} = arg\ \min_{\boldsymbol{w}} E$. By assuming $\boldsymbol{w} = \widehat{\boldsymbol{w}}$ when $t = t_e$, thus $\boldsymbol{w}(0) - \widehat{\boldsymbol{w}} = -\int_0^{t_e} \alpha\, \boldsymbol{z} \otimes \boldsymbol{x}\, dt$ when $t = t_e$, and $\boldsymbol{w}(t) - \widehat{\boldsymbol{w}} = -\int_t^{t_e} \alpha\, \boldsymbol{z} \otimes \boldsymbol{x}\, dt$. Although $\boldsymbol{w}$ and $\widehat{\boldsymbol{w}}$ were not directly measured experimentally, the relative deviation of $\boldsymbol{w}$ from $\widehat{\boldsymbol{w}}$ can be derived from $\boldsymbol{x}$ and $\boldsymbol{z}$ signals recorded in the SNIC experiments,

$$\Delta\boldsymbol{w}(t) = \frac{\boldsymbol{w}(t)-\widehat{\boldsymbol{w}}}{|\boldsymbol{w}(0)-\widehat{\boldsymbol{w}}|} = -\frac{\int_t^{te} \alpha\, \boldsymbol{z} \otimes \boldsymbol{x}\, dt}{\left|\int_0^{te} \alpha\, \boldsymbol{z} \otimes \boldsymbol{x}\, dt\right|} \approx -\frac{\int_t^{te} \boldsymbol{z} \otimes \boldsymbol{x}\, dt}{\left|\int_0^{te} \boldsymbol{z} \otimes \boldsymbol{x}\, dt\right|} \tag{S2}$$

In the human experiments, $\boldsymbol{x}$ and $\boldsymbol{y}$ signals were recorded, $\boldsymbol{z}$ was derived from $\boldsymbol{y}$ based on Equation S1, and the effective $\Delta\boldsymbol{w}$ was also derived from Equation S2.

In the self-programming process, the change of $\boldsymbol{w}$ leads to the change of output signals $\boldsymbol{y}$, which modifies the objective function E. Without loss of generality, the objective function E can be expressed as,[2]

$$E = \frac{1}{2}\boldsymbol{g}^{E/\boldsymbol{w}} \circ \Delta\boldsymbol{w}^2 + \delta[\Delta\boldsymbol{w}^3] \tag{S3}$$

where $\boldsymbol{g}^{E/\boldsymbol{w}} \circ \Delta\boldsymbol{w}^2$ denotes the Hadamard product between $\boldsymbol{g}^{E/\boldsymbol{w}}$ and $\Delta\boldsymbol{w}^2$ with $\boldsymbol{g}^{E/\boldsymbol{w}} \in \mathbb{R}^{N\times M}$ and $\boldsymbol{g}^{E/\boldsymbol{w}} \geq 0$, and $\delta[\Delta\boldsymbol{w}^3]$ contains higher order terms of $\Delta\boldsymbol{w}^k$ with $k \geq 3$. When $\Delta\boldsymbol{w}$ approaches zero, $\delta[\Delta\boldsymbol{w}^3]$ can be omitted, and the average E over a self-programming period, $\langle E\rangle \approx \frac{1}{2}\langle \boldsymbol{g}^{E/\boldsymbol{w}} \circ \Delta\boldsymbol{w}^2\rangle = \frac{1}{2}g^{E/\boldsymbol{w}}\langle\Delta\boldsymbol{w}\rangle^2 + \frac{1}{2}g^{E/\boldsymbol{w}}\langle\Delta\widetilde{\boldsymbol{w}}\rangle^2 = \frac{1}{2}g^{E/\boldsymbol{w}}\langle\Delta\boldsymbol{w}\rangle^2 + E_{eq}$, which was best-fitted by the experimental data of $\langle E\rangle$ and $\Delta\boldsymbol{w}$ to extrapolate $g^{E/\boldsymbol{w}}$ and E_{eq}, and displayed in Figure 3 and 4.

In the self-programming process, $\boldsymbol{w}$ is modified by following Equation 2, $\dot{\boldsymbol{w}} = \alpha\, \boldsymbol{z} \otimes \boldsymbol{x}$. By substituting $\boldsymbol{z}$ in Equation 2 by $\boldsymbol{z} = \boldsymbol{y} * \tilde{\theta}$ Equation 4, $\dot{\boldsymbol{w}} = \alpha\,(\tilde{\theta} * \boldsymbol{y}) \otimes \boldsymbol{x}$. In neuron circuits, $\boldsymbol{y}$ is a monotonically increasing nonlinear function of $\boldsymbol{I}$, and $\boldsymbol{I} = \boldsymbol{w}\,\boldsymbol{x}$ Equation 1, thus $\boldsymbol{y} = \boldsymbol{y}(\boldsymbol{I}) = f^{y}(\boldsymbol{w}\boldsymbol{x})$. By substituting $\boldsymbol{y}$ in $\dot{\boldsymbol{w}}$ by $\boldsymbol{y}(\boldsymbol{w}\boldsymbol{x})$, $\dot{\boldsymbol{w}} = \alpha[\tilde{\theta} * \boldsymbol{y}(\boldsymbol{w}\boldsymbol{x})] \otimes \boldsymbol{x}$, and the modification rate of $\Delta\boldsymbol{w}$ over a self-programming period[2],

$$\Delta\dot{\boldsymbol{w}} = -\boldsymbol{\beta} \circ \Delta\boldsymbol{w} + \delta\boldsymbol{w} \qquad \text{(S4)}$$

where $\boldsymbol{\beta} \circ \Delta\boldsymbol{w}$ denotes the Hadamard product between $\boldsymbol{\beta}$ and $\Delta\boldsymbol{w}$ with $\boldsymbol{\beta} \in \mathbb{R}^{N\times M}$ and $\boldsymbol{\beta} \geq 0$, and $\delta\boldsymbol{w}$ contains the higher order terms of $\Delta\boldsymbol{w}^k$ with $k \geq 2$ and $\dot{\hat{\boldsymbol{w}}}$. $\Delta\boldsymbol{w}$ can be extrapolated based on Equation S2, and $\boldsymbol{\beta}$ can be derived by best-fitting $\Delta\boldsymbol{w}$ and $\Delta\dot{\boldsymbol{w}}$ to Equation S4. The derived β are shown versus $\langle\Delta\dot{w}\rangle$ at the initial self-programming state in Figure 4a. The solution of Equation S4 gives,

$$\Delta\boldsymbol{w} = \Delta\boldsymbol{w}(0)e^{-\boldsymbol{\beta}t} + \delta\boldsymbol{w} * e^{-\boldsymbol{\beta}t} \qquad \text{(S5)}$$

where $\delta\boldsymbol{w} * e^{-\boldsymbol{\beta}t}$ represent the convolution between $\delta\boldsymbol{w}$ and $e^{-\boldsymbol{\beta}t}$. When $\boldsymbol{\beta}t \gg 1$, $\langle\Delta\boldsymbol{w}\rangle \approx 0$, and $\langle\boldsymbol{w}\rangle \approx \langle\hat{\boldsymbol{w}}\rangle$, thus $\boldsymbol{\beta}$ represents the speed to modify $\boldsymbol{w}$ toward $\hat{\boldsymbol{w}}$.

In the self-programming process, the change of $\boldsymbol{w}$ leads to the change of the objective function E. Based on Equation S3, the change rate of average objective function $\langle\dot{E}\rangle = \boldsymbol{g}^{E/\boldsymbol{w}} \circ \langle\Delta\boldsymbol{w} \circ \Delta\dot{\boldsymbol{w}}\rangle + \delta[\Delta\boldsymbol{w}^2 \circ \Delta\dot{\boldsymbol{w}}] + \left.\frac{\partial\langle E\rangle}{\partial t}\right|_{\Delta\boldsymbol{w}}$. Substituting $\Delta\dot{\boldsymbol{w}}$ in $\dot{E}$ by Equation S4 yields, $\langle\dot{E}\rangle = -g^{E/\boldsymbol{w}} \circ \boldsymbol{\beta} \circ \langle\Delta\boldsymbol{w}^2\rangle + \delta[\Delta\boldsymbol{w}^2 \circ \Delta\dot{\boldsymbol{w}}] + \left.\frac{\partial\langle E\rangle}{\partial t}\right|_{\Delta\boldsymbol{w}} = -\frac{1}{2}\beta g^{E/\boldsymbol{w}} \circ \langle\Delta\boldsymbol{w}^2\rangle + \delta[\Delta\boldsymbol{w}^3] + \left.\frac{\partial\langle E\rangle}{\partial t}\right|_{\Delta\boldsymbol{w}} = -\beta\langle E\rangle + \delta E$ (Equation 3), where $\beta = \sum_{m,n} 2\langle\beta_{nm}\rangle/MN \geq 0$, $\delta E = \delta[\Delta\boldsymbol{w}^3] + \left.\frac{\partial\langle E\rangle}{\partial t}\right|_{\Delta\boldsymbol{w}}$ contains higher order terms of $\Delta\boldsymbol{w}^k$ with $k \geq 3$, and $\left.\frac{\partial\langle E\rangle}{\partial t}\right|_{\Delta\boldsymbol{w}}$ due to environmental perturbations. When δE satisfies $\delta E < \beta\langle E\rangle$, then $\langle\dot{E}\rangle < 0$, $\langle E\rangle$ represents a Lyapunov function and is asymptotically decreased, $\boldsymbol{w}$ is modified toward $\hat{\boldsymbol{w}}$, and $\Delta\boldsymbol{w}$ toward zero. When $\langle E\rangle$ is reduced to make $\beta\langle E\rangle = \delta E$, $\langle\dot{E}\rangle = 0$, $\langle E\rangle$ reaches a dynamic equilibrium value $E_{eq} = \delta E/\beta$. When $\langle\Delta\boldsymbol{w}\rangle$ approaches zero, $\delta\,(\Delta\boldsymbol{w}^3)$ can be omitted, $\langle E\rangle \approx \frac{1}{2}\langle\boldsymbol{g}^{E/\boldsymbol{w}} \circ \Delta\boldsymbol{w}^2\rangle = \frac{1}{2}g^{E/\boldsymbol{w}}\langle\Delta\boldsymbol{w}\rangle^2 +$

$\frac{1}{2}g^{E/w}\langle\Delta\widetilde{\boldsymbol{w}}\rangle^2 = \frac{1}{2}g^{E/w}\langle\Delta\widetilde{\boldsymbol{w}}\rangle^2 = E_{eq}$. E_{eq} increases with increasing $\langle\Delta\widetilde{\boldsymbol{w}}^2\rangle$ due to the random perturbation from environment and the fluctuation of $\boldsymbol{w}$ during the self-programming process, as shown in Figure 4b. When $\langle\Delta\boldsymbol{w}\rangle$ descends to zero, $\langle E\rangle \approx \frac{1}{2}g^{E/w}\langle\Delta\widetilde{\boldsymbol{w}}\rangle^2 = E_{eq}$, as shown in Figure 3 and 4.

The self-programming process of a SNIC and neurobiological network is summarized in the following theorem,[2]

Theorem 1. When a SNIC or neurobiological network (i) concurrently executes the signal processing algorithm $\boldsymbol{I} = \boldsymbol{w}\,\boldsymbol{x}$ (Equation 1), and the correlative learning algorithm $\dot{\boldsymbol{w}} = \alpha\,\boldsymbol{z} \otimes \boldsymbol{x}$, (Equation 2) with $\boldsymbol{z} = \boldsymbol{y} * \tilde{\theta}$ (Equation S1); (ii) when $\boldsymbol{w} = \widehat{\boldsymbol{w}}$, $\boldsymbol{F} = \widehat{\boldsymbol{F}}$, $\boldsymbol{x} = 0$, then $\dot{\boldsymbol{w}} = 0$, and $\widehat{\boldsymbol{w}}$ represents the equilibrium value of $\boldsymbol{w}$; (iii) when $\boldsymbol{w} = \widehat{\boldsymbol{w}}$, the objective function $E = \frac{1}{2}(\boldsymbol{F} - \widehat{\boldsymbol{F}})^2 = 0$; when $\boldsymbol{w} \neq \widehat{\boldsymbol{w}}$, $\boldsymbol{F} \neq \widehat{\boldsymbol{F}}$, and $E > 0$, then in the self-programming process, $\langle\dot{E}\rangle = -\beta\langle E\rangle + \delta E$ (Equation 3) with $\beta > 0$; (iv) When δE satisfies $\delta E < \beta\langle E\rangle$, then $\langle\dot{E}\rangle < 0$, $\langle E\rangle$ represents a Lyapunov function, and is asymptotically decreased, leading $\boldsymbol{w}$ to be modified toward $\widehat{\boldsymbol{w}}$ in the self-programming process; (v) when $\delta E = \beta\langle E\rangle$, $\langle\dot{E}\rangle = 0$, $\langle E\rangle$ reaches its dynamic equilibrium value $E_{eq} = \delta E/\beta$.

An integrate-and-fire "neuron" circuit

We designed and fabricated an integrate-and-fire circuit with the basic functions according to the Hodgkin–Huxley neuron model[3]. The "neuron" circuit is shown in Figure S6a. The collective current, I, from multiple synstors flows through a diode toward a capacitor C_{IF}, increasing the voltage, V_C, on the capacitor. A negative voltage, V_L, is applied to induce a leakage current, I_L, flowing through the resistor, R_L, to filter the thermodynamic and signal noises in the circuits. V_C is proportional to the integration of $I - I_L$ with respect to time. When V_C reaches a threshold value, a Schmitt trigger composed of transistors M1-M6 is switched back and forth to generate an output pulse from the output channel, V_f. The output pulse resets V_C

back to zero by switching transistors M7, M8, and M9, and the capacitor C_{IF} restarts the integration of the current. A "neuron" circuit with $C_{IF} = 9.4$ nF, $R_L = 50\ M\Omega$, $V_L = -0.15\ V$, and $R_{INV} = 0.25\ M\Omega$ was tested by applying a series of 10 ns-wide input pulses to inject a current I to C_{IF}. The firing rates of output voltage pulses triggered from an output neuron circuit, r_y, are plotted versus the firing rates of input voltage pulses applied on a synstor, r_x, in Figure S6b. r_y can be expressed as,

$$r_y = \frac{r_y^{max}}{1+e^{-k_y(I-I_L)}} = \frac{r_y^{max}}{1+e^{-k_y(wV_p t_d r_x - I_L)}} \qquad \text{(S6)}$$

where the maximal saturation value of r_y, $r_y^{max} = 6.01\ kHz$, I denotes the current flowing into the integrate-and-fire neuron circuit with $I = wV_p t_d r_x$, w denotes the synstor conductance, the magnitude of input voltage pulses $V_p = 1.75\ V$, the duration of input voltage pulses $t_d = 10$ ns, the leakage current from the integrate-and-fire neuron circuit, $I_L = 0.44\ nA$, and the fitting parameter $k_y = 7.81\ /nA$, when the synstor is modified to its high conductance with $w = 10\ nS$, or low conductance with $w = 0.1\ nS$.

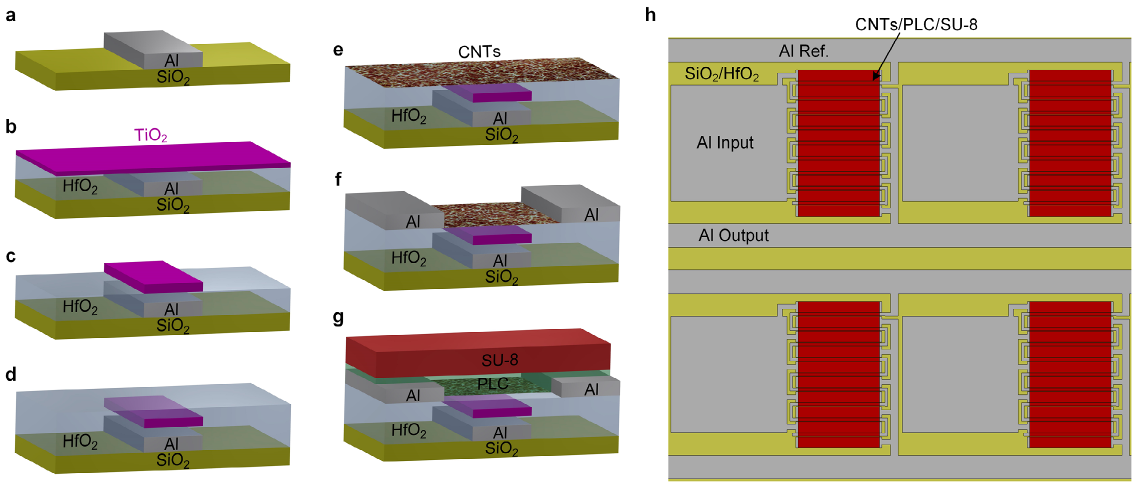

Figure S1. a) A 50 nm thick and 10 µm long Al reference electrode (gray) is deposited onto the 100 nm thick SiO_2 layer (yellow) of an Si/SiO_2 wafer by electron beam (e-beam) evaporation, and patterned by photolithography and wet chemical etching. b) A 22 nm thick HfO_2 dielectric barrier layer (clear blue) and a 2 nm thick TiO_2 charge storage layer (magenta) are deposited by atomic layer deposition (ALD). c) The TiO_2 charge storage layer is patterned by photolithography and reactive ion etching (RIE) with a 10 µm long pattern aligned to the Al reference electrode. d) A 6.5 nm thick HfO_2 barrier layer is deposited by ALD, encapsulating the TiO_2 charge storage layer. e) A randomly oriented semiconducting single-walled carbon nanotube (CNT) network channel (orange) is deposited by wet immersion coating from an aqueous solution of 99.9% pure semiconducting CNTs. f) 50 nm thick Al input and feedback electrodes (gray) are deposited by e-beam evaporation, and patterned by photolithography. g) A 200 nm thick passivation layer of parylene-C (clear green) is deposited by thermal evaporation. An encapsulation and patterning layer of SU-8 photoresist (red) is deposited by spin-coating, patterned by photolithography, and used as an etch mask to etch the parylene-C and CNT layers with RIE to form a 20 µm long CNT channel. h) A top-view of a 2 × 2 crossbar synstor circuit with the labeled locations of the CNT channel covered by the parylene-C (PLC) passivation and SU-8 photoresist layers (red), the input, output, and reference electrodes (gray).

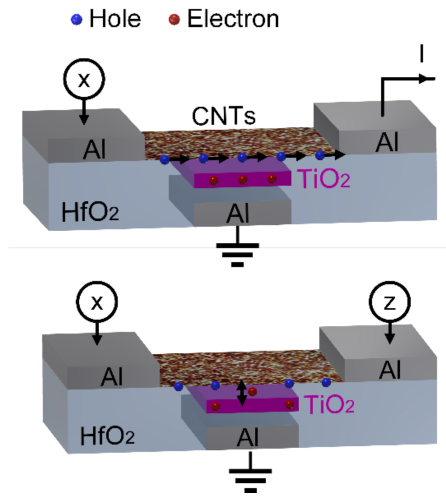

Figure S2. The synstor is composed of Al input and output electrodes (gray), a randomly oriented semiconducting single-walled carbon nanotube (CNT) network channel (orange), HfO_2 dielectric layers (blue-gray), a TiO_2 charge storage layer (magenta), and an Al reference electrode (gray). A voltage pulse is applied to the input electrode x to induce a current flowing through the CNT channel on the output electrode, while the output and reference electrodes are grounded. Charge in the TiO_2 storage layer modulates the density of holes in the p-type doped CNT channel, controlling the channel conductance w and current I flowing across the CNT layer on the output electrode. When voltage pulses x and z with the same amplitude are simultaneously applied to the input and output electrodes with respect to the grounded reference electrode, current across the channel $I = 0$, and electrons hop through the HfO_2 dielectric layer between the CNT channel and TiO_2 charge storage layer, modifying the charge in the TiO_2 layer and channel conductance w.

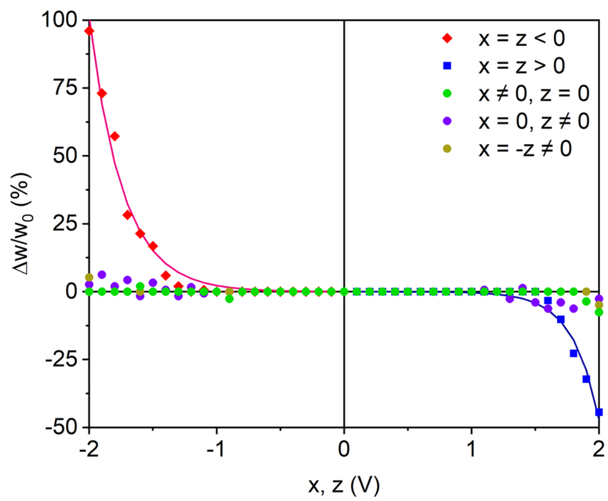

Figure S3. Relative changes of a synstor conductance $\Delta w/w_0$ induced by 50 pairs of various 5 ms-wide x and z voltage pulses applied on the input and output electrodes of the synstor are plotted versus the pulse amplitudes. The $\Delta w/w_0$ data are fitted by $\Delta w/w_0 = e^{\mu^+(x-x_t^+)} - 1$ (magenta line) when $x = z > V_t^+$ with $\mu^+ = 4.06/V$ and $x_t^+ = 1.05\ V$, and $\Delta w/w_0 = e^{-\mu^-(x-x_t^-)} - 1$ (blue line) when $x = z < V_t^-$ with $\mu^- = 3.69/V$ and $x_t^- = -0.81\ V$. The w is modified by following Equation 2, $\dot{w} = \alpha\ z \cdot x$. When $x = z \gtrsim 1.0\ V$, w was decreased ($\alpha < 0$); when $x = z \lesssim -0.8\ V$, w was increased ($\alpha > 0$); when $-0.8\ V \lesssim x = z \lesssim 1.0\ V$, $\dot{w} \approx 0$ ($\alpha \approx 0$). $|\alpha|$ increases with the increasing magnitude of $|x|$ and $|z|$. The synstor conductance does not change under $xz = 0$.

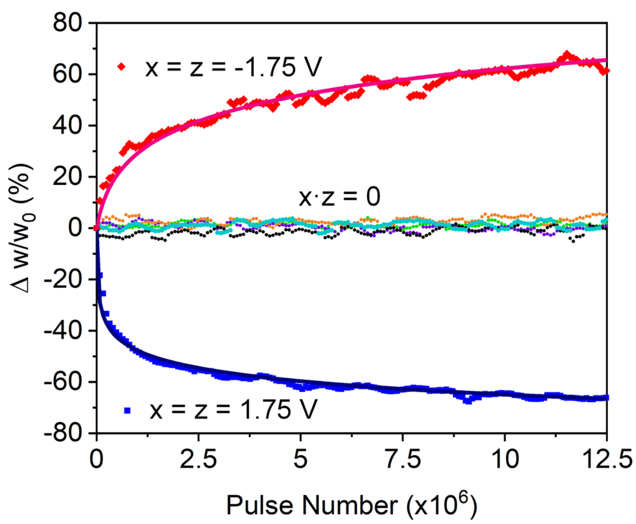

Figure S4. Cumulative relative changes of synstor conductance $\Delta w/w_0$ are displayed versus cumulative numbers, n, of 10 ns-wide x and z voltage pulses applied to the input and output electrodes of the synstor under the voltage amplitudes of $x = z = -1.75\ V$ (red diamonds), $x = z = 1.75\ V$ (blue squares), $x = z = 0$ (black), $x = 1.75\ V$ and $z = 0$ (green), $x = 0$ and $z = 1.75\ V$ (purple), $x = 0$ and $z = -1.75\ V$ (orange), $x = -1.75\ V$ and $z = 0$ (turquoise), respectively. The $\Delta w/w_0$ data are best-fitted by $\Delta w(n)/w_0 = \nu^- Ln\left(\frac{n}{n_0^-} + 1\right)$ with $\nu^- = 15.3$ and $n_0^- = 1.76 \times 10^5$ under $x = z = -1.75\ V$ (magenta lines), and $\Delta w(n)/w_0 = \nu^+ Ln\left(\frac{n}{n_0^+} + 1\right)$ with $\nu^+ = 7.5$ and $n_0^+ = 1.7 \times 10^3$ under $x = z = 1.75\ V$ (dark blue lines). The synstor conductance increases versus increasing n under $x = z = -1.75\ V$, decreases versus increasing n under $x = z = 1.75\ V$, otherwise, the synstor conductance does not change under $xz = 0$.

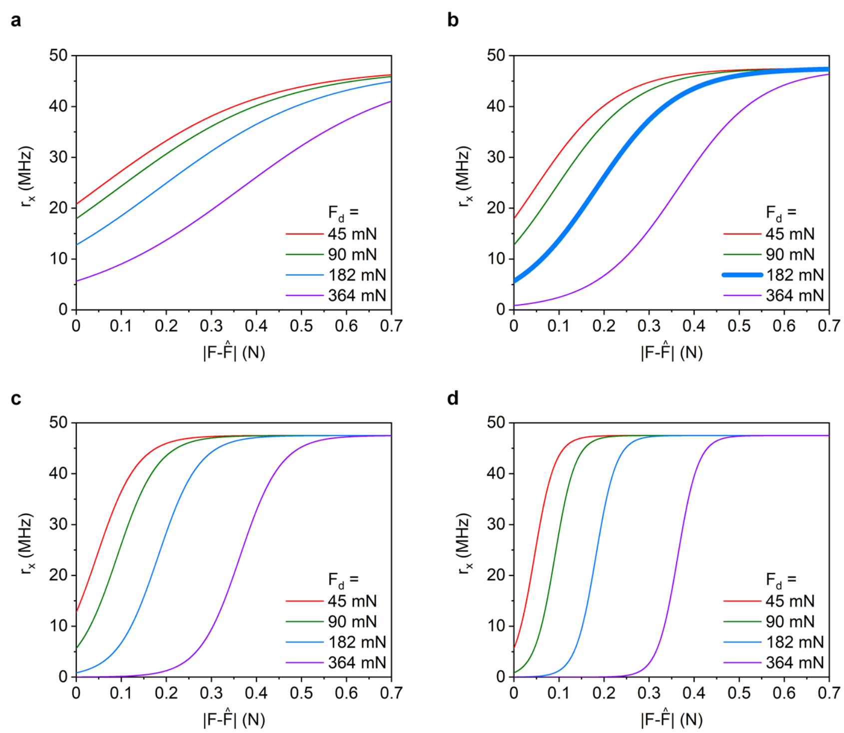

Figure S5. The firing rates of input pulses to a synstor circuit, r_x, are plotted versus $|F - \hat{F}|$ by following $r_x = \frac{r_x^{max}}{1+e^{-k_x(|F-\hat{F}|-F_d)}}$, where F denotes the experimentally measured lift-force on a wing, the targeted value of the lift-force, $\hat{F} = 0.3\ N$, the maximal saturation value of r_x, $r_x^{max} = 47.5\ Mhz$, the parameter $F_d = F_d^0$ (red), $2F_d^0$ (green), $4F_d^0$ (blue), or $8F_d^0$ (purple) with $F_d^0 = 45.5\ mN$, and the parameter a) $k = k_x^0$, b) $k = 2k_x^0$, c) $k = 4k_x^0$, and d) $k = 8k_x^0$ with $k_x^0 = 5.5\ N^{-1}$. The minimal objective function E is achieved under $F_d = 4F_d^0$ and $k = 2k_x^0$ (bold blue line) in b.

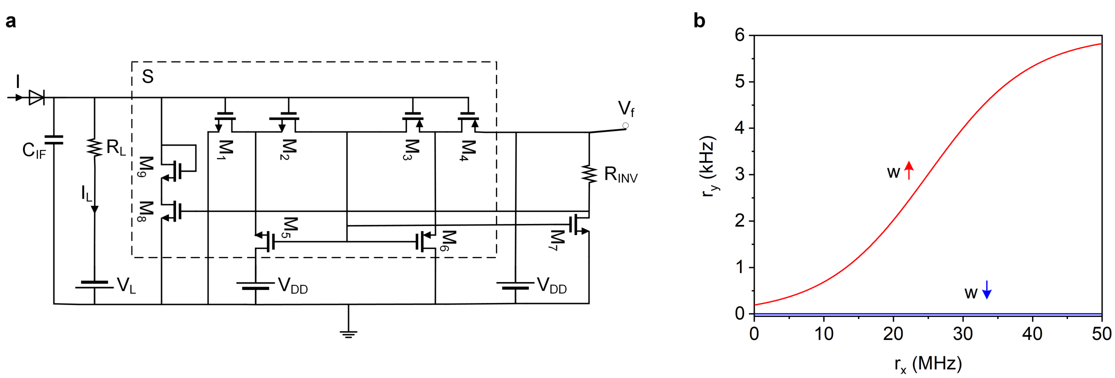

Figure S6. a) The integrate-and-fire "neuron" circuit consists of a capacitor, C_{IF}, a diode, two resistors, R_L and R_{INV}, and nine Si CMOS transistors (M_1-M_9). b) The firing rates of output voltage pulses triggered from an output neuron circuit, r_y, are plotted versus the firing rates of input voltage pulses applied on a synstor, r_x, when the synstor is modified to its high conductance with $w = 10\ nS$ (red line), or low conductance with $w = 0.1\ nS$ (blue line).

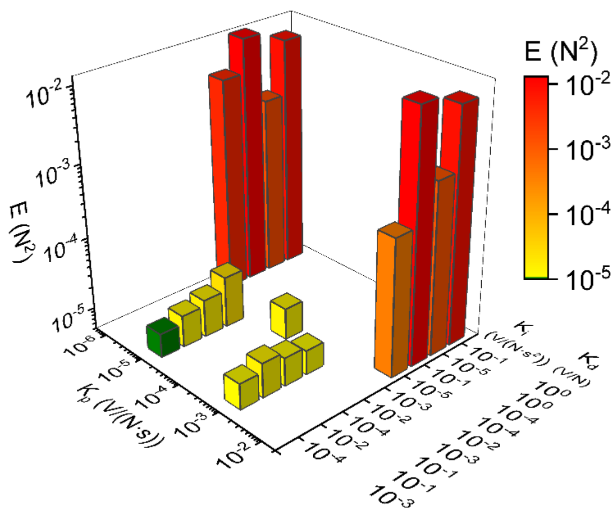

Figure S7. The average objective function $\langle E \rangle = \frac{1}{2}\langle (F - \hat{F})^2 \rangle$ during PID control processes of a morphing wing in a wind tunnel with a wind speed $S \approx 29\ m/s$ is shown versus the the proportional gain K_p, the integral gain K_i, and the derivative gain K_d of the PID controller. $\langle E \rangle$ approaches its minimal value (green) under the optimal gains with $K_p = 10^{-5}\ V/N \cdot s$, $K_i = 10^{-4}\ V/N \cdot s^2$, and $K_d = 10^{-3}\ V/N$.

References

[1] Y. Dan, M.-M. Poo, *Neuron* **2004**, *44*, 23.

[2] Y. Chen, *Advanced Intelligent Systems* **2020**, 2000219.

[3] A. L. Hodgkin, A. F. Huxley, *The Journal of Physiology* **1952**, *117*, 500.